Astron. Astrophys. 341, 740–750 (1999)

ASTRONOMY AND ASTROPHYSICS

# Complex variability pattern in NGC 4151

## II. Variable absorption features

**S.G. Sergeev**[1,2], **V.I. Pronik**[1,2], **E.A. Sergeeva**[1,2], **and Yu.F. Malkov**[1]

[1] Crimean Astrophysical Observatory, P/O Nauchny, 334413 Crimea, Ukraine
[2] Isaac Newton Institute of Chile, Crimean Branch

Received 17 July 1998 / Accepted 14 October 1998

**Abstract.** We found and identified the blueshifted variable absorption features in the NGC 4151 optical spectra obtained in 1992–1996. Two of these features identified with He I $\lambda$4471 and $\lambda$7065 lines have been investigated in detail. The most striking change in the He I $\lambda$4471 equivalent width was its strengthening between ≈JD2450212–JD2450315. We present some indications of the extremely low-ionization state of absorber in this period of observations. We do not find clear evidence for a correlation (neither inverse nor direct) of equivalent widths with the state of the nucleus activity. This probably means that strong changes in the covering factor (or something else) affect this correlation. The decomposition method based on the different behavior of broad emission lines and absorption lines allows us to separate these spectral features, and to obtain evidence that the H$\alpha$, H$\beta$ and H$\gamma$ absorption lines are also present. The presence of the absorption lines cause the variations of the broad emission profiles to become more complicated. Possible explanations for the absorption variability are discussed.

**Key words:** galaxies: Seyfert – galaxies: quasars: emission lines – galaxies: quasars: absorption lines – galaxies: nuclei – galaxies: individual: NGC 4151 – galaxies: active

### 1. Introduction

The presence of an absorption feature near $\lambda$3880 Å in the spectrum of the NGC 4151 nucleus was first noted by Mayall (1934), however the regular purposeful studying of it begins only when Anderson & Kraft (1969), following the suggestion of Wilson (see Oke & Sargent 1968), attributed the $\lambda$3880 Å absorption feature to a detail of the He I $\lambda$3889 P Cygni-like profile. Anderson & Kraft (1969) also showed blueshifted absorption lines in the wings of the Balmer line emission. Later the single spectra observed at different times by different authors (Anderson & Kraft 1971; Cromwell & Weymann 1970) led to conclude that absorption lines can change their position in the spectrum and their strength within a time span of 30 days or less. The most detailed description of the observations available earlier and their interpretation is in the paper of Anderson (1974).

*Send offprint requests to*: S.G. Sergeev (sergeev@crao.crimea.ua)

An intensive study of the ultraviolet absorption lines and their variability has been carried out by Bromage et al. (1985). They concluded that these lines must arise in several different locations but not in material emitting the broad lines. The study of the numerous ultraviolet absorption features performed by Kriss et al. (1992) leads to the conclusion that the absorbing region consists of many clumps of dense material ($n_e \geq 10^{9.5} cm^{-3}$) with internal velocities within each cloud of $\sim 200$ km s$^{-1}$. The most detailed study of a structure of ultraviolet absorption lines based on a small-scale monitoring program at high resolution and high $S/N$ ratio has been carried out by Weymann et al. (1997). They found a large number of separate components in C IV and Mg II, and set limits on the amount of secular acceleration or deceleration of the C IV absorption system which shows no evidence for any change in velocity of the components over a span of nearly 4 years. One component of the Mg II absorption complex has been seen for over 15 years and was first claimed by Leech et al. (1987, 1991). Although the gross features of the absorption complexes have changed remarkable little, it was found that a high-velocity transient absorption component and large changes in absorption strength of Si IV have been seen from the last observational epoch.

There is also a question whether the absorption lines are related to the so called X-ray warm absorber (Nandra & Pounds 1992). Low-ionization species in NGC 4151 present a problem in attempting to place both absorbers in the same material (Kriss et al. 1995).

As was noted by Anderson (1974), the He I $\lambda$3889 absorption seems to have been continually present with relatively little change in strength since it was first noted by Mayall in 1934, while the Balmer absorption features during the same interval changed their width and depth noticeably. In this respect we should like to note that the depression in the Balmer line profiles does not yet mean that absorption is present. It is well known that the shapes of the broad-line profiles in AGNs are complex and strongly variable (Peterson 1993; Sergeev et al. 1994). An emission detail (a bump) on the wing of the broad-line profile can mimic an absorption feature between this bump and the profile center, which is especially dangerous at the low spectral resolution typically used to study the broad emission lines in AGNs.

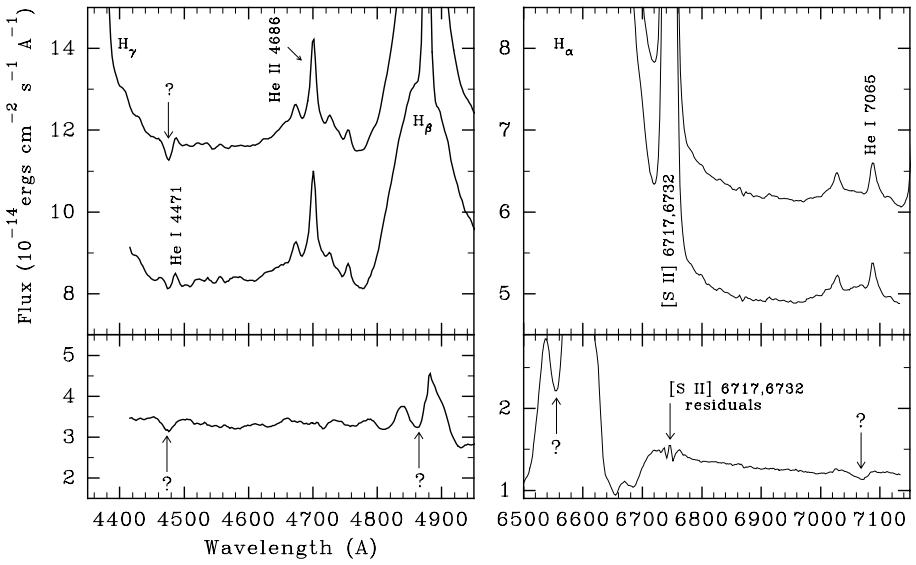


**Fig. 1.** The mean of NGC 4151 spectra obtained in November 1991–August 1995 (*lower spectrum*) is compared with the mean of spectra obtained in October 1995–December 1996 (*upper spectrum*). The residuals with clearly visible absorption features at $\lambda$4476 and $\lambda$7071 are plotted in the *lower panels*. The wavelengths are given in the observer frame.

Unfortunately, the He I $\lambda$3889 is outside the CCD frames of our spectra. In the present paper we study mostly the variation of the much weaker He I $\lambda$4471 and He I $\lambda$7065 absorption lines. The He I $\lambda$4471 strengthened in 1996. We paid attention to it because this wavelength region was used to fit the continuum (Malkov et al. 1997, Paper I). Strongly different behavior of He I $\lambda$4471,$\lambda$7065 absorption lines and Balmer emission lines led us to obtain the absorption features separately from the Balmer emission lines, assuming all available absorption lines are varying in phase. Based on this separation we can confirm that the Balmer absorption is really present. However, the detailed study of this absorption is strongly limited by the changes in the profile shape of Balmer emission lines.

## 2. Observations and data processing

Our spectral monitoring of NGC 4151 has been carried out in the Crimean Astrophysical Observatory on the 2.6-m Shajn telescope since 1988. The spectra were registered on CCD in the two separate spectral regions near the H$\alpha$ and H$\beta$ lines. In the previous paper (Paper I) the instrumentation and data processing have been described in detail. In the present paper we will analyze the spectra obtained in November 1991–December 1996. Spectra that were obtained since August 1995 have not been used in Paper I. They include 61 individual spectra in the H$\alpha$ region and 45 in the H$\beta$ region or 51 and 41 respectively if nightly averaged. We have also a single spectrum obtained between the H$\alpha$ and H$\beta$ spectral regions, and containing the He I $\lambda$5875 line.

## 3. Absorption features

### *3.1. The preliminary identification*

In Paper I, we selected two zones at 4465–4495 Å and 5095–5140 Å (observer frame) to fit the continuum near H$\beta$ line. However, our new observations performed since August 1995 show that the blue zone at 4465–4495 Å has an absorption feature and is not suitable as continuum zone. This feature is clearly visible in Fig. 1, where the mean of the old spectra is compared with the mean of the new spectra, and the residuals are plotted below. The apparent central wavelength of the absorption is 4476 Å. To be sure that this feature is not an artifact, we have studied carefully all possible sources of errors. We have checked that there are no bad pixels (with non-linear response) near that position on CCD, no telluric lines at that wavelength and no similar absorption features at the same wavelength in other AGNs (with different redshifts) observed in the same period. This absorption can also not be produced by the host galaxy because it is variable in flux as can see from the residuals in Fig. 1. Thus this feature must belong to the NGC 4151 nucleus.

In the same manner we examined the H$\alpha$ region spectra. The residuals between the mean of the old spectra and the mean of the new spectra clearly show the absorption feature at $\lambda$7069 (Fig. 1). The spectral region near this absorption is relatively free from telluric lines. The redward and blueward spectral regions have much more prominent molecular lines ($H_2O$, $O_2$, OH), but the residuals shown in Fig. 1 do not contain any features at those regions. This proves that both the emission and absorption telluric lines were correctly removed from our spectra as described in Paper I.

The numerous absorption features observed in NGC 4151 (Anderson 1974; Bromage et al. 1985; Kriss et al. 1992; Weymann et al. 1997) are generally blueshifted relative to the frame of NGC 4151 by 700–1200 km s$^{-1}$, thus their observed velocities are close to zero because the NGC 4151 has a redshift of about 940 km s$^{-1}$. If so, it is easy to identify the absorption features at $\lambda$4476 and $\lambda$7069 with the He I $\lambda$4471 and $\lambda$7065 lines. Both lines are formed with the transitions from the same level ($2^3P - 4^3D$ and $2^3P - 3^3S$ respectively).

From Fig. 1 it is also seen that the residuals of the H$\beta$ and H$\alpha$ line profiles have a double-peaked structure which can be interpreted as an absorption feature superposed on the single-peaked broad emission profile. The presence of the Balmer absorption lines has been noted first by Anderson & Kraft (1969).

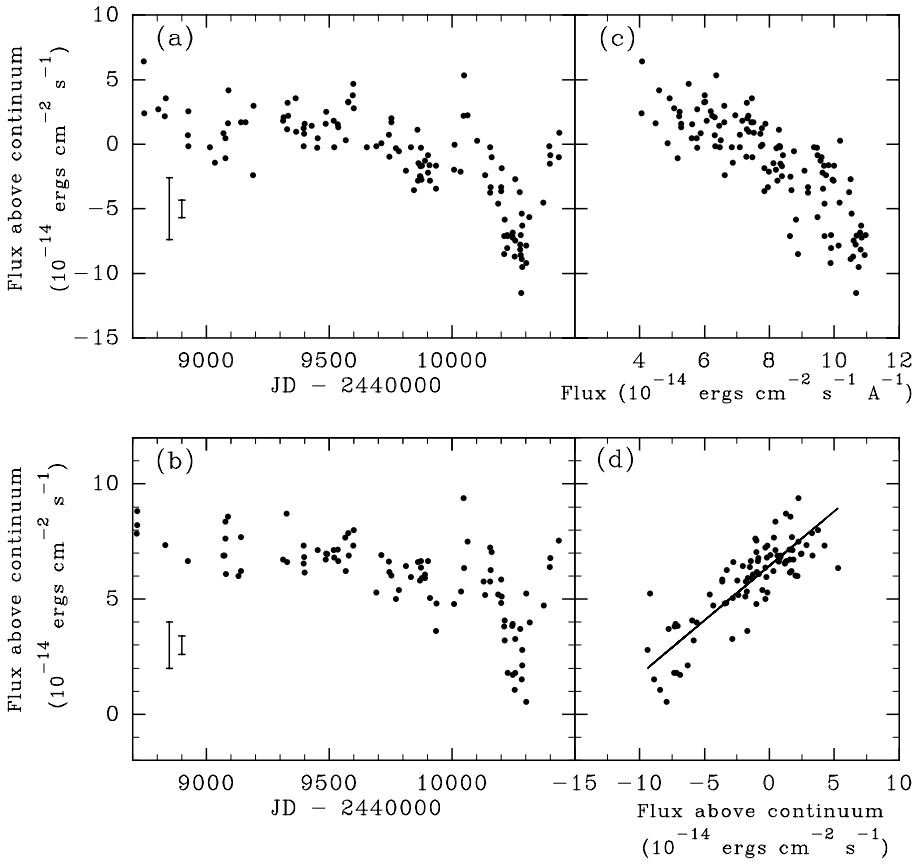


**Fig. 2a–d.** The light curves of the He I $\lambda$4471 and $\lambda$7065 absorption lines are shown in **a**,**b**. A negative value of the flux means that the absorption dominates the narrow emission. The two vertical bars are the largest and smallest error of individual measurements. **c** shows the relation between the He I $\lambda$4471 absorption line flux and the continuum flux. The relation between the He I $\lambda$4471 and $\lambda$7065 absorption line fluxes is shown in **d**.

The identification of these lines and their study is limited by the changes in shape of the broad emission profiles. So, one can ask whether the double-peaked residuals in Fig. 1c,d are caused by the strengthening of the Balmer absorption lines or by the changes in the Balmer emission profiles. The evidence in favor of the Balmer absorption lines is their blueshift relative to the systematic velocity of NGC 4151. Further evidence will be presented in the following sections.

### *3.2. The light curves*

The primary reason why we need the light curves of He I $\lambda$4471 and $\lambda$7065 absorption lines is to utilize them in the decomposition method described in Sect. 3.3. With this decomposition method we will be able to look for other absorption features and to estimate the contribution of the narrow emission to the He I $\lambda$4471 absorption line. Next we will obtain the He I $\lambda$4471 equivalent width in each spectrum. To measure the absolute fluxes in the He I $\lambda$4471,$\lambda$7065 absorption lines the nightly averaged spectra have been used. We have estimated the noise value in each spectrum near the target lines, discarding the H$\beta$ region spectra with noise greater than $1.7 \cdot 10^{-15}$ ergs cm$^{-2}$ s$^{-1}$ Å$^{-1}$ and the H$\alpha$ region spectra with noise greater than $7.5 \cdot 10^{-16}$ ergs cm$^{-2}$ s$^{-1}$ Å$^{-1}$. Under a such criterion for data quality, a total of 120 H$\beta$ region spectra and 92 H$\alpha$ region spectra were used. Selecting the absolute noise value instead of the signal-to-noise ($S/N$) ratio we have set an upper limit of absolute error of our measurements. We have fit the continuum by a straight line, using the redward and blueward zones near each line. The zones have been chosen at 4448–4460 Å, 4494–4513 Å for He I $\lambda$4471 and 7038–7049 Å, 7105–7125 Å for He I $\lambda$7065. We did not remove the weak narrow emission superposed on the absorption lines to get the light curves to be free from a method of such removal. Due to the contribution of the narrow emission in the continuum zones the fitted continuum can be slightly overestimated, so the measured flux in the absorption line will be overestimated also. However, the presence of the same He I lines in emission as well as other narrow lines (Sect. 3.4, Fig. 5) must reduce the measured value. The flux has been calculated by direct integration of straight lines connecting individual data points (at the zones of 4460–4495 Å and 7049–7100 Å respectively) and assumed positive if the function value is above the continuum and negative otherwise. Due to the noise in the original spectra and the presence of the same He I lines and other narrow lines in emission (Sect. 3.4, Fig. 5) the resulting value can be positive as well as negative. The negative value means, of course, that there are many data points below the continuum, so the absorption dominates the emission. Since the narrow emission lines are not variable such a method of measurement can only shift the real line light curve but its shape must remain the same. We have verified this obvious assumption by removing these lines from our spectra using the [O III] $\lambda$5007 profile as a template and measuring the flux of the net absorption line (Sect. 3.4). In Fig. 2a,b the light

curves of the He I $\lambda$4471 and $\lambda$7065 absorption lines are shown. In Fig. 2d the dependence between the line fluxes obtained by rebinning the He I $\lambda$4471 line light curve to the times of observations of the He I $\lambda$7065 line light curve is shown. It is easy to see that both lines vary similarly. The slope of the regression line (the two most deviated points were omitted) in Fig. 2d of $0.472 \pm 0.031$ gives the ratio of the line fluxes. To get the ratio of the equivalent widths, it is necessary to know the relationship of the non-stellar continuum fluxes near those lines (the broad line contribution is negligible). We have obtained the dependence between the fluxes at the narrow continuum bands centered on $\lambda$6967 Å and $\lambda$4500 Å, using pairs of measurements obtained within the same nights of observations. The double-weighted linear regression gives the slope of this dependence of $0.439 \pm 0.006$, which can be interpreted as the ratio of the non-stellar continuum fluxes ($F_{6967}/F_{4500}$). Thus the ratio of equivalent widths is $W_{7065}/W_{4471} = 1.08 \pm 0.07$. Without the rebinning of the He I $\lambda$4471 light curve, but only selecting the quasi-simultaneous pairs (the observations within the same nights), the double-weighted regression gives $W_{7065}/W_{4471} = 1.24 \pm 0.08$.

If the equivalent width of these lines was constant during the period of observations, a linear dependence between the line absolute flux and the continuum flux must exist. Perhaps, this is not the case as can be seen from Fig. 2c.

We have calculated the error for each individual measurement of the line fluxes. In Fig. 2a,b only the largest and the smallest error bars ($2\sigma$) are shown, while the individual errors are not shown to avoid the obstruction of picture. The errors for the individual measurements were calculated using a Monte-Carlo simulation. Random Gaussian deviates consistent with the errors in a given observed spectrum were added to the average spectrum and the fluxes of the target lines were measured. The above procedure was repeated many times. The errors in the original spectra were estimated using the deviation of the flux at each pixel from the average flux at the two neighboring pixels. If the values deviated too much (more than $3\sigma$), then such pixels were omitted and the next iteration done. The final root mean square deviation (RMSD) must be greater by factor of $\sqrt{1.5}$ than the error per pixel we are interested in.

### *3.3. The decomposition of spectra*

To obtain the net profile shape of the He I $\lambda$4471,$\lambda$7065 lines we have used the decomposition algorithm described by Sergeev et al. (1994, 1997). Let us assume the series of spectra contains a fixed number of variable components with non-variable shapes. If the light curves of the components are known (it does not matter if the light curves are transformed linearly) then the shapes of the components can be obtained by solving the linear least squares problem. The solution of this problem gives a system of normal equations:

$$\sum_i S_i(\lambda) cov(L_i(t), L_j(t)) = cov(F(\lambda, t), L_j(t)) \qquad (1)$$

where $t = t_1, t_2, \ldots, t_n$ are the times of the observations, $L_i(t)$ is the known light curve of the $i$-th component, $\lambda = \lambda_1, \lambda_2, \ldots, \lambda_k$ is a series of wavelengths over which the spectra are rebinned, $F(\lambda, t)$ is the observed fluxes in our series of spectra, the $cov$ is a covariance function of two time series and $S_i(\lambda)$ is the unknown shape of the $i$-th component. In matrix form a set of Eq. (1) can be written as:

$$x(\lambda)A = b(\lambda) \qquad (2)$$

where $A$ is a matrix with the elements $A_{ij} = cov(L_i(t), L_j(t))$, $x(\lambda)$ is a vector of the unknown shapes of components at wavelength $\lambda$, and $b(\lambda) = cov(F(\lambda, t), L_j(t))$ is a vector of constants. Inverting Eq. (2) at each wavelength we obtain the profile shapes of the components:

$$x(\lambda) = b(\lambda)A^{-1} \qquad (3)$$

To obtain the profile shapes of the He I $\lambda$4471,$\lambda$7065 lines it is only necessary to know their light curves, because no other variable features are present near those wavelengths except the weak broad emission of the same He I lines and the continuum which can be subtracted easily from the resulting components. The decomposition gives a result very similar to that of the residuals shown in Fig. 1. Next we have tried to separate the H$\alpha$ and H$\beta$ absorption lines from the same broad emission lines. We have assumed a second component with the light curve of the H$\alpha$ and H$\beta$ broad emission lines. Preparing the light curve of this component to be implemented in the Eq. (1) we have calculated the fluxes of the H$\alpha$ and H$\beta$ broad emission lines only at the two narrow zones located approximately at $-2600\,\mathrm{km\,s^{-1}}$ and $+800\,\mathrm{km\,s^{-1}}$. Thus, we have excluded the spectral region where the presence of the absorption line is suspected (otherwise the light curve will be mixed with the absorption component) and only include the regions which are close to the absorption position. In Fig. 3 the obtained components are shown. The two upper panels show the spectral component that varies similar to the He I $\lambda$4471,$\lambda$7065 absorption lines, while the lower panels show the component that varies similar to the H$\alpha$ and H$\beta$ broad emission lines. Unfortunately, the first component is contaminated with the residuals of the broad line profiles which have not been separated correctly, because their profile shapes vary, while Eq. (1) is only correct if the profile shape is steady. The residuals of the He II $\lambda$4686 broad line profile in Fig. 3a are caused, in addition, by different behavior of this line and of the broad Balmer lines (Paper I). The continuum in Fig. 3 has no physical meaning, it does not vary like either the broad Balmer lines or the absorption features, so it cannot be related to only one of these components. Thus we must be careful with the identification of any absorption feature in Fig. 3a,b when it is superposed on the broad line profiles. We have paid attention only to the most prominent features identified with the Balmer absorption lines. We have also examined the spectral regions were the contribution of the broad lines is negligible. Excepting already known He I $\lambda$4471,$\lambda$7065 absorption lines we have found a weak but significant absorption feature at $\lambda$5176. This feature can be identified with the Mg I $\lambda$5167, $\lambda$5172, $\lambda$5183 or Fe II $\lambda$5169. We did not find evidence for the presence of other absorption lines of Fe II, so the identification with the

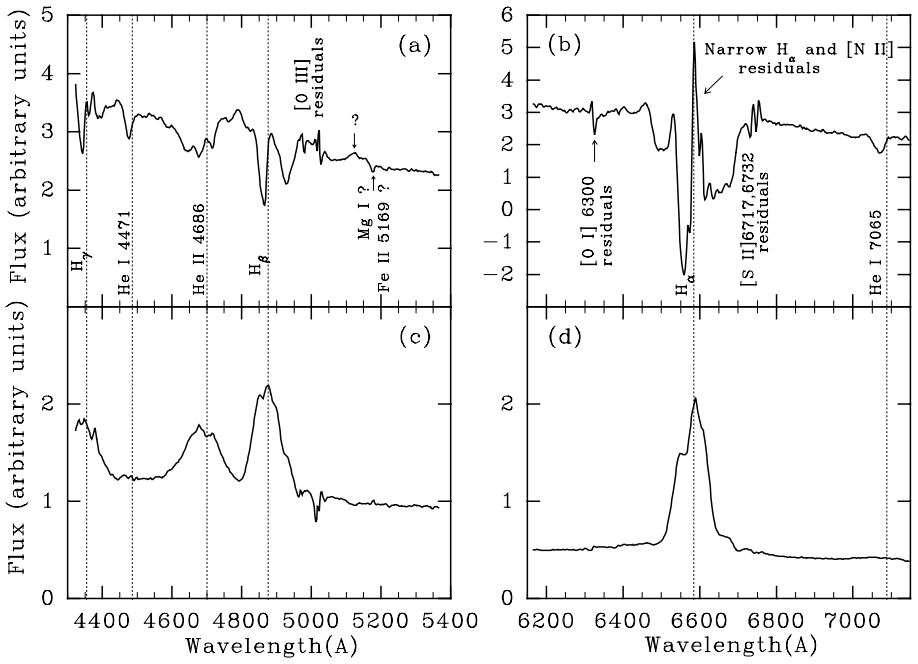


**Fig. 3a–d.** Spectral decomposition applied to a set of our spectra as described in the text. **a** and **b** show the component that varies similar to the He I $\lambda$4471,$\lambda$7065 absorption lines, while **c** and **d** show the component that varies similar to the H$\alpha$ and H$\beta$ broad emission lines. The absorption component has residuals of the broad line profiles which have not been separated correctly, because their profile shapes vary. However, most prominent absorption features can be identified with the Balmer lines. The wavelengths are given as observed. Vertical dotted lines show the positions of some spectral lines.

Mg I multiplet seems to be more probable, and suggests extremely low-ionization species definitely related to the nucleus. The flux of the non-variable (in equivalent width) absorption lines must strictly follow the continuum light curve and only relates to the spectral component varying in the same way as the continuum. Using our decomposition method, we have verified that the $\lambda$5176 absorption feature is completely absent in the continuum-related component, but only visible in the component varying in the same way as He I $\lambda$4471. Table 1 gives a centroid and FWHM of identified absorption features (the He I $\lambda$5875 and Na I $\lambda$5890, $\lambda$5896 absorption lines will be discussed separately). The centroid has been measured below the half maximum level and is given in km s$^{-1}$ units relative to the nucleus and in Å units in the observer frame. The radial velocity of the nucleus was adopted to be equal to 940 km s$^{-1}$. In most cases, the widths of the absorption lines are 2.5 times greater than the instrumental profile width. The resolution of individual spectra may differ due to the focusing and seeing quality. Before applying the decomposition facilities, we have adjusted the resolution of our spectra (see Sergeev et al. 1997; Malkov et al. 1997). We estimated that the adjusted resolution is equal to 9 Å in all spectral regions. It means that the resolution in velocity units is 560 km s$^{-1}$ near the H$\beta$ line and 410 km s$^{-1}$ near the H$\alpha$ line.

The Balmer absorption lines have a blueshift and width very similar to those of He I $\lambda$4471 and $\lambda$7065. Some differences in the radial velocities of He I lines and the Balmer lines (Table 1) can be attributed to the uncertainties in the separation of the absorption component from the broad emission lines of the Balmer series. There may also be physical reasons for such a difference.

In Fig. 4 the profile shapes of the He I $\lambda$4471,$\lambda$7065 absorption lines from Fig. 3a,b are compared separately in velocity units relative to the nucleus. Both profiles seem to be very similar confirming our identification of these lines. The strange feature is an emission bump at $\approx -2500$ km s$^{-1}$, prominent in the profiles of both lines. It is not clear what this emission feature means which becomes brighter when the absorption is deeper. Similar behavior is shown by a bump marked in Fig. 3a with a question mark. Although this bump is not pronounced in the individual spectra, it is well seen in the residuals of spectra. We have calculated the light curve of this bump and compared its behavior with the behavior of the equivalent width of the He I $\lambda$4471 absorption line obtained as described in Sect. 3.4. Although the curves seem to be slightly different, the correlation coefficient equals 0.57, while the correlation coefficient between the bump light curve and continuum light curve is only 0.19.

**Table 1.** Parameters of the absorption lines found

| Identification | Centroid[a] | | FWHM[b] | Equivalent width[c] |
|---|---|---|---|---|
| | (Å) | (km s$^{-1}$) | (km s$^{-1}$) | (Å) |
| H$\gamma$ | 4339.8 | −990 | 1270 | 1.55 (1.22) |
| He I $\lambda$4471 | 4475.2 | −690 | 1450 | 0.99 (0.99) |
| H$\beta$ | 4861.0 | −960 | 1440 | 3.09 (1.84) |
| Mg I?[d] | 5176.1 | | 750 | 0.27 (0.27) |
| He I $\lambda$5875 | | | | 1.88 (1.68) |
| Na I $\lambda$5890,96? | | | | 1.49 (1.34) |
| H$\alpha$ | 6559.3 | −1100 | 1540 | 11.0 (2.90) |
| He I $\lambda$7065 | 7070.2 | −730 | 1290 | 1.23 (1.18) |

[a] The wavelength is given in the observer frame, while the velocity is given relative to the nucleus.
[b] The instrumental profile has an FWHM of 9 Å.
[c] Obtained assuming two situations: the absorber covers (1) only the continuum source and (2) both the continuum source and BLR.
[d] Multiplet lines $\lambda$5167,5172,5183

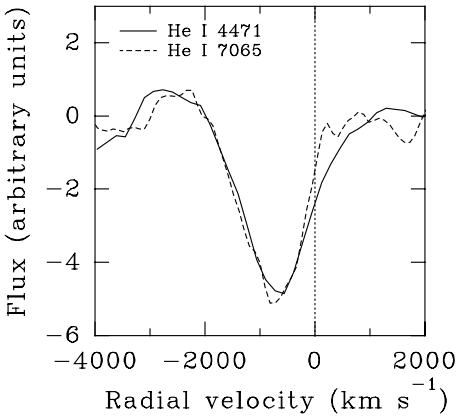


**Fig. 4.** The profile shapes of He I $\lambda$4471 and $\lambda$7065 absorption lines from Fig. 3a,b are compared. The velocity is given in the frame of the nucleus. The scaling in flux is arbitrary.

The separated broad Balmer profiles in Fig. 3c,d (especially the H$\alpha$ line) still show some sign of absorption. The contamination with the absorption component can be explained by the different behavior of Balmer absorption lines and He I $\lambda$4471. It can be caused by the different physical conditions in individual clouds as well as by the saturation in the curve-of-growth of H$\alpha$ line. Moreover, the broad-line region (BLR) and the optical continuum source probably have significantly different geometrical sizes, so the absorber must cover different fractions of those regions. The He I $\lambda$4471,$\lambda$7065 absorption lines are formed by absorbing the continuum emission, while the Balmer absorption lines are formed by absorbing the emission from both the small continuum region and the more extended BLR.

As was mentioned above the absorption component in Fig. 3a,b is contaminated by the residuals of the broad lines (generally the Balmer lines and He II $\lambda$4686). To reduce these residuals we have performed more complex decomposition assuming that the emission Balmer line profiles consist of two or more components. Assumption of a two-component model of broad-emission profiles reduces the residuals of the broad Balmer lines, but they are still present and do not disappear after addition of the third, and even fourth emission component. The following conclusions have been drawn:

1. The variations of the profile shapes of broad emission lines are extremely complicated. It is very difficult to separate weak absorption features superposed with those profiles.
2. The light curve of Balmer lines at $V \approx -1000$ km s$^{-1}$ is significantly different from the light curves at any other regions of the profile. It can not be fitted with any linear combination of light curves at any other velocities.
3. We did not find other He I lines ($\lambda$4387, $\lambda$4921, $\lambda$6678). That means that either these lines are weak or hidden with the variations of profile shapes of broad lines. The He I $\lambda$4713 absorption line is probably present but so contaminated with the He II $\lambda$4686 broad emission profile that it can not be measured unambiguously.

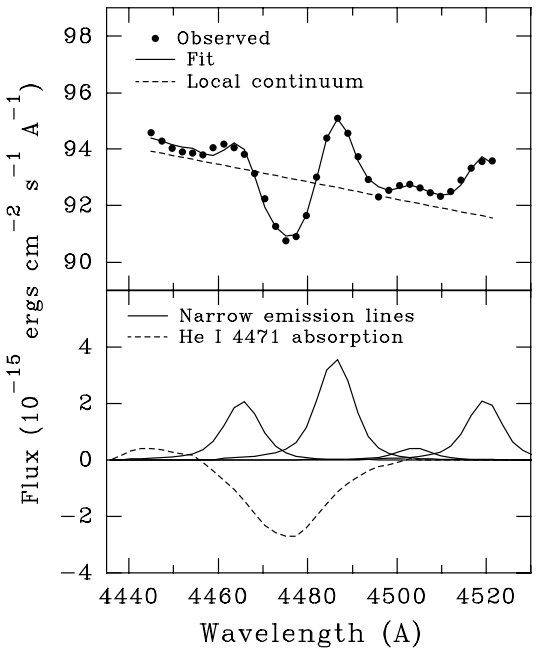


**Fig. 5.** Fitting the average spectrum with a sum of the narrow lines, the He I $\lambda$4471 absorption line and the continuum. The wavelengths are given in the Observer's frame.

### *3.4. The equivalent widths*

To measure the equivalent width (EW) of the He I absorption lines it is necessary to remove the narrow emission features. The He I $\lambda$4471 absorption line is not as strongly contaminated by the narrow emission lines as He I $\lambda$7065. We have removed the narrow emission features from the He I $\lambda$4471 absorption profile by fitting the average spectrum with a sum of the narrow lines, the absorption line and the local continuum. The [O III] $\lambda$5007 line profile was used as a template for the narrow lines, the profile of absorption was taken as derived in the previous section, and the continuum was taken to be a straight line. Minimizing the Root Mean Square Deviation (RMSD) between the modeling spectrum and the observed spectrum we have fitted the observed spectrum as shown in Fig. 5. We have estimated the signal-to-noise ratio per pixel ($S/N$) in each spectrum near the target line. Since the measurement error in EW is proportional to $S/N$ we have therefore set its lower limit discarding the spectra with $S/N < 70$. We have subtracted the sum of the narrow lines from each spectrum. Next we have measured the EW, using the same wavelength zones as in Sect. 3.2. The measured EWs were corrected for the stellar contribution. In Paper I, we estimated that the stellar contribution at $\lambda$5120 through our entrance aperture is $1.0 \cdot 10^{-14}$ ergs cm$^{-2}$ s$^{-1}$ Å$^{-1}$. If so, the linear regression between the continuum fluxes at $\lambda$5120 and 4500 yields a value of $7.6 \cdot 10^{-15}$ ergs cm$^{-2}$ s$^{-1}$ Å$^{-1}$ for the stellar contribution at $\lambda$4500. The corrected EW values are only 9% greater (on average) than the original values, so the influence of the stellar contribution is nearly negligible. The result of the measurements of EW is present in Fig. 6. It is clearly visible that the He I $\lambda$4471 absorption is variable in EW. During

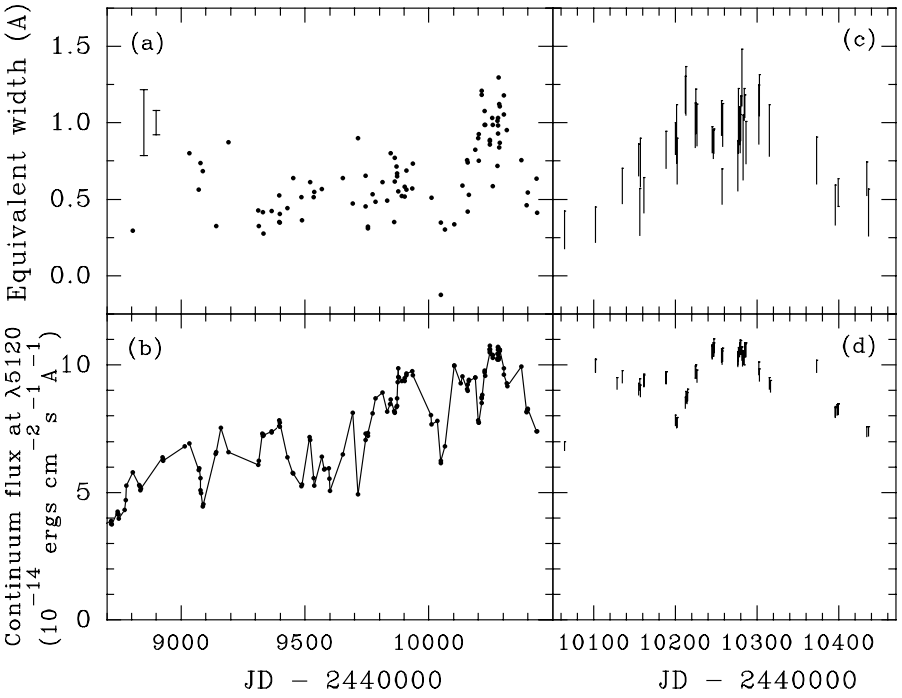


**Fig. 6a–d.** Equivalent width of the He I $\lambda$4471 absorption line after removing the narrow emission lines **a**, its behavior during a short period when the variations were apparently more pronounced **c** and the light curve of the optical continuum at $\lambda$5120 **b**,**d**.

the period ≈JD2450212–JD2450315 it becomes approximately twice as strong as was found in the preceding period.

Having the EW of the He I $\lambda$4471 absorption line, we calculated the EWs of other absorption features. We have directly measured the relative fluxes of the absorption lines in Fig. 3a,b and estimated the non-stellar continuum intensity nearby these lines as well as the contribution from the underlying BLR emission. The fluxes of the H$\beta$ region absorption features (H$\beta$, Mg I) were compared with the flux of He I $\lambda$4471, while the flux of the H$\alpha$ absorption line was compared with the flux of He I $\lambda$7065. Since the EW ratio of the He I $\lambda$7065 and $\lambda$4471 lines has already been estimated in Sect. 3.2 ($W_{7065}/W_{4471} = 1.24 \pm 0.08$), we have obtained the EWs of all absorption lines relative to He I $\lambda$4471. Table 1 gives the measured values of the EWs. They are related to the epoch when the absorption was extremely high (≈JD2450212–JD2450315, see Fig. 6), so the He I $\lambda$4471 absorption line has an EW of 0.99 Å. In the preceding period the EW of the He I $\lambda$4471 absorption line was less by factor of 2. Two values of EW in Table 1 have been obtained assuming two cases: the absorber covers the continuum source only (while the BLR emission is only an additive background), and the absorber covers both the continuum and BLR. The last value is enclosed in parenthesis.

We have also estimated the EW of He I $\lambda$5875 absorption line (the same series as $\lambda$4471 and $\lambda$7065 lines) which is clearly visible in a spectrum from the period when the absorption was extremely high (JD=2450214.42). No more spectra have been obtained in this spectral region. The direct measurement of EW is impossible due to the presence of broad and narrow emission lines (Fig. 7a). However, the EW of the He I $\lambda$5875 absorption line can be roughly estimated by fitting the absorption and narrow emission features (Fig. 7b) to obtain the smoothest residuals

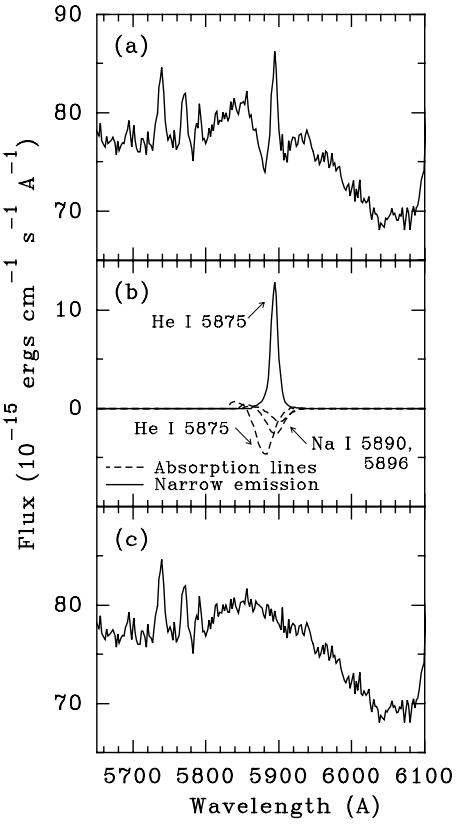


**Fig. 7a–c.** The observed spectrum with the broad, narrow and absorption lines of He I $\lambda$5875 is shown in **a**. The absorption and narrow emission lines in **b** were adjusted so (see also text) that the residuals in **c** are smooth and can be treated as a net broad line.

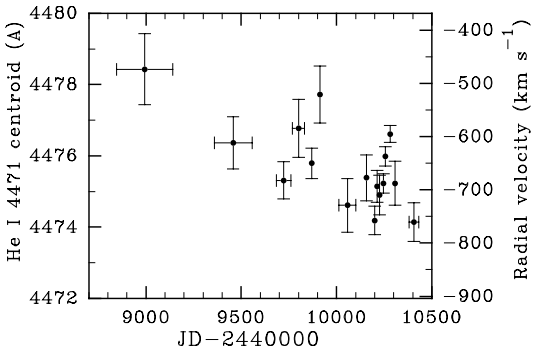


**Fig. 8.** Changes in the centroid of the He I $\lambda$4471 absorption line profile. The horizontal error bars denote the RMSD of the Julian Dates of averaged spectra, while the vertical errors bars were derived from the Monte-Carlo simulation. The velocity-axis is given relative to the nucleus.

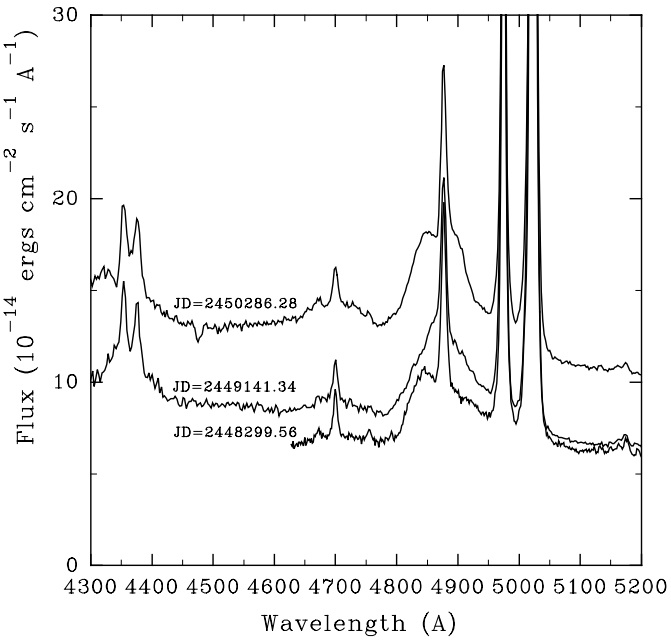


**Fig. 9.** Examples of some spectra of NGC 4151. The wavelengths are given as observed.

when these features are subtracted from the original spectrum (Fig. 7c). The profile of the He I $\lambda$4471 absorption line and the profile of the [O III] $\lambda$5007 emission line have been taken as templates. We have also fitted the absorption feature redwards of the He I $\lambda$5875 narrow line, attributed to the Na I $\lambda$5896,$\lambda$5890 absorption lines. But a greater number of spectral lines means a greater number of free parameters. Therefore, we have reduced the number of free parameters assuming that the radial velocities and widths of absorption features are the same as those of the He I $\lambda$4471 absorption line. We have also set the ratio of Na I $\lambda$5896,$\lambda$5890 lines to 1:1 (large saturation case). The EWs of He I $\lambda$5875 and Na I $\lambda$5896,$\lambda$5890 are given in Table 1. The assumption of no saturation (ratio 2:1) gives very similar result. Next we performed a fit assuming the Na I is entirely related to the Galaxy and NGC 4151, but not to the nucleus. In this case, the fit is unphysical (with the Galaxy component in emission) and its quality is worse. We concluded that at least some of the Na I absorption can be attributed to the nucleus.

Finally we applied this "classic" decomposition method to the Balmer lines in order to compare its result with the result of our method described in Sect. 3.3. We have failed to fit unambiguously the H$\alpha$ line (where the [N II] narrow emission is an additional contaminator), but the H$\beta$ and H$\gamma$ absorption lines were reasonably separated. Their measured EWs are larger by 40% than the EWs given in Table 1. Taking into account that the unknown shape of the BLR emission is a notoriously difficult problem the agreement of 40% can be treated as reasonable.

### *3.5. The changes in the radial velocity of* He I *$\lambda$4471 absorption*

Subtracting the narrow emission features as described in the previous section, it is possible to measure the centroid of the He I $\lambda$4471 absorption. Unfortunately, the individual spectra (excluding the period when the equivalent width of absorption was large) has a noise comparable with the depth of this line. Thus we need to average many spectra to get the centroid with a reasonable error value. In Fig. 8 the centroid measurements are presented. The horizontal error bars denote the RMSD of the Julian Dates of averaged spectra and the vertical error bars were derived from the Monte-Carlo simulation. It can be suspected that the line centroid has shifted systematically to the higher velocity during the period of observations. During a short period when the absorption was extremely high (≈JD2450212–JD2450315), the centroid has shifted gradually to the lower velocity. The only systematic effect that can alter the apparent radial velocity is an incorrect estimation of the contribution of the narrow lines. We have checked that the long-term trend mentioned above can be removed with different changes in the narrow line fluxes by 15–30%, while the short-term trend can not. All our attempts to suppress the short-term trend by varying the narrow line fluxes have led to a significant strengthening of the long-term trend. In our opinion, the changes in radial velocity are most likely real and caused by the changes in relative strength of the components of the complex absorption line.

### *3.6. The absorption and the broad-line profile "bumpiness"*

The observed profiles of the broad H$\beta$ line in NGC 4151 have a blue bump near the line center. Sometimes, this bump is very prominent as can be seen from Fig. 9, where examples of some spectra of NGC 4151 are shown. A possible explanation of appearance of such bump is an absorption H$\beta$ line superposed on the broad-emission line profile. Taking the ratio of fluxes in two bins of the H$\beta$ line profile as a criterion of the bumpiness, there is a direct correlation between this criterion and the EW of He I $\lambda$4471 (Fig. 10).

So far we have not mentioned the NGC 4151 spectra obtained in February 1988–March 1991 and referred to as "Cassegrain" spectra (Paper I). One of these spectra (nightly av-

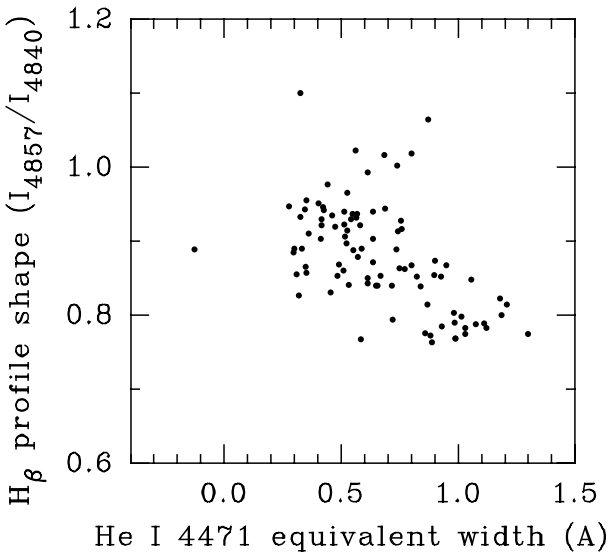


**Fig. 10.** The dependence between the criterion of the H$\beta$ line profile "bumpiness" (the ratio of fluxes in two bins of the H$\beta$ line profile) and the equivalent width of the He I $\lambda$4471 line. It can be seen that the blue bump is more prominent when the He I $\lambda$4471 absorption line is stronger.

eraged) is the bottom spectrum in Fig. 9. Unfortunately, we can not say anything about the He I $\lambda$4471,$\lambda$7065 absorption lines at this early period of observations, because most Cassegrain spectra do not cover the wavelengths where these absorption lines are observed. The H$\beta$ line profile in the Cassegrain spectrum in Fig. 9 has a prominent blue bump. The residuals between this spectrum and the spectrum obtained in the period when this bump has been less prominent do not show any sign of an absorption-like feature in the H$\beta$ broad line profile. Probably, the blue bump in the H$\beta$ broad-line profile of the Cassegrain spectra (the bottom spectrum in Fig. 9) is mostly an intrinsic property of the emission-line profile. On the contrary, the blue bump of the H$\beta$ broad line profile in the upper spectrum in Fig. 9 is most likely driven by the strengthening of the absorption features in this observation period.

## 4. Discussion

The EW of the absorption lines formed by absorbing the direct emission of the continuum source (and BLR) by the clouds in the line-of-sight only depends on the population of a lower level ($n_i$) and the oscillator strength ($f_{ji}$): $W_{ij} \sim n_i \lambda B_{ij} \sim n_i \lambda_{ij}^2 f_{ji}$ (assuming no saturation, i.e. $\tau \ll 1$ even in the line center). The He I $\lambda$4471, $\lambda$4713, $\lambda$7065 and $\lambda$5875 lines originate from the same atomic level. Adopting $gf_{4471} = 1.12$, $gf_{4713} = 0.106$, $gf_{7065} = 0.624$ and $gf_{5875} = 5.48$ the ratio of equivalent widths will be as follows: $W_{7065}/W_{4471} = 1.38$, $W_{5875}/W_{4471} = 8.45$ and $W_{4713}/W_{4471} = 0.11$. The first ratio is in reasonable agreement with the observed value (Table 1), while the second ratio is much greater. The weak He I $\lambda$4713 absorption line is superposed on the He II $\lambda$4686 broad emission profile and can not be measured unambiguously. Examining the $W_{H_\alpha}/W_{H_\beta}$ and $W_{H_\beta}/W_{H_\gamma}$ observed ratios, they appear to be much lower than predicted, which is evidence in favor of saturation in the curve-of-growth. Although the observed absorption lines seem to be not too deep, the line depth in individual clouds can be large enough. So, at higher resolution, these lines must show a complex structure with several deep and narrow components, probably the same as claimed by Weymann et al. (1997). We have checked that the profile shape of He I $\lambda$4471 (Fig. 4) can be satisfactorily fitted by summing our instrumental profiles with the radial velocities of components $A, C$ and $E/E'$ of Weymann et al., while adding the component $D$ does not improve the $\chi^2$-criterion. However, the result of the fit shows that these components must be still slightly resolved at our spectral resolution, so a real line structure can be more complex and include more components.

A very weak line identified (but not firmly) with the Mg I multiplet has a width only a little greater than the instrumental profile width and probably consists mostly of a single component belonging to one of the multiplet lines. Its EW (Table 1) yields a column density of $6 \cdot 10^{12} cm^{-2}$ (without saturation), but the column density of the same atoms in the ground state must be definitely higher. So, the Mg I column density related to the period when the absorption has been extremely high is even larger than the column density of Mg II derived by Weymann et al. (1997) for the earlier epochs. Such low-ionization species may suggest the strong changes in the ionization state of absorbing clouds. Inspection of IUE spectra of NGC 4151 obtained in December 1993 shows no evidence for the presence of the Mg I $\lambda$2852 absorption line at ground level, while the Mg II multiplet is present. Thus either our identification is completely wrong or the ionization state of the absorber has decreased significantly. The strengthening of observed absorption features can be a result of such a decrease.

Examining the EW behavior of the He I $\lambda$4471 absorption line it can be noted that the most significant change is its strengthening for a short period of observations, shown in detail in Fig. 6c. We have checked whether any changes in the EW have been observed for the earlier period (JD$\leq$2450102) and found only one data point (JD=2450048) which deviated by 5.3$\sigma$ from the mean value for this period. If this point is discarded, there is no further evidence for variations and $\chi^2$ =53 per 53 degree of freedom (d-o-f), while for the entire period of observations it equals 309 per 92 d-o-f. So, the variations, if any, were not detectable within our measurement errors and only pronounced for the period of observations shown in Fig. 6c. It is clearly seen that the EW has increased, then decreased, then increased again, and finally returned almost to its initial state. This complex event has been seen for a span of about 250 days, while the total observational period is about 6.5 times longer. It probably means we have observed a rather unique event which can not be seen often. In our opinion, such a rare event can be driven either by the appearance of new material (a cloud moving across the line-of-sight) or by the changes in the shielding of the absorbing clouds from the ionizing radiation of the central source (probably caused by the BLR clouds). Now we discuss the reasons for the observed absorption variability.

*A new cloud in the line-of-sight.* The increase in the EW (Fig. 6) has been observed during a period $\Delta t \sim$100 days which can be treated as the time span needed for a cloud moving across the line-of-sight to cover a distance equal to its size. Unfortunately, we do not know the transverse component of the cloud velocity ($V_t$), but we can suppose that $V_t \ll V_r$, where $V_r \approx 700\,\mathrm{km\,s^{-1}}$ is the radial velocity. Then the cloud size can be estimated as $r \ll V_t \Delta t$, i.e. $r \ll 0.2$ l.d. Such a cloud cannot cover the BLR significantly, but only the optical continuum source the size of which must be comparable to or less than the cloud size to provide strong changes in the EW. A new cloud passing the line-of-sight must introduce a new component into many absorption lines and thus the observed correlation between the He I and Balmer lines (Fig. 3,Fig. 10) can be explained easily. However, the strengthening of a new component must displace systematically the radial velocity of an entire absorption line. Although changes in the centroid of He I $\lambda$4471 has been seen (Fig. 8), they do not correlate with the EW. We have also examined the changes in the line width, which is found to have varied only by 7% (root mean square variations, taking into account the measurement errors) and again, no correlation with the EW was found. Thus the observed picture can be explained only in the terms of at least two clouds. Although there are indeed two maxima in the EW variations (Fig. 6c), the nearly simultaneous passage of two clouds seems to be hardly probable.

*Changes in the ionizing radiation.* Another reason of absorption variability is the variation of ionizing radiation emitted toward the observer (along the line-of-sight) and driven either by the nucleus activity or by the changes in the covering factor in this direction. The EWs of different species belonging to different absorbing clouds may show an inverse or direct correlation with the ionizing flux. For the low-ionization species one can rather expect the inverse correlation, although it is not so obvious and depend on the physical conditions in a given cloud, the examined species and levels and the shape of the ionizing spectrum. In some cases, the influence of the non-ionizing radiation can also be important. However, the same correlation with the optical continuum will only be observed if the covering factor (of BLR clouds) and the continuum slope do not vary. We do not know exactly whether the optical continuum properly represents the behavior of the ionizing continuum or if the broad emission lines do that better. Therefore, we have calculated correlation coefficients between the EWs of the He I $\lambda$4471 absorption line and both the optical continuum fluxes and the broad H$\beta$ line fluxes separately for the entire period of observations and only for the period (shown in Fig. 6c), when the variations were apparently more pronounced. The time delay in the changes of the H$\beta$ broad line relative to the optical continuum is probably less than 10 days (Maoz et al. 1991; Kaspi et al. 1996; Malkov et al. 1997). To evaluate numerically how a lag can affect our result we have considered two cases: there is no delay and there is a delay of 10 days. The calculated coefficients are shown in the first two rows of Table 2. Now, let us consider a situation in which the covering factor is strongly variable, but changes more slowly than the ionizing radiation driven by the nucleus activity. Obviously, a link of the EW with the optical continuum will only be pronounced for such a time span for which the covering factor does not vary significantly. We have filtered all the curves (both EWs and fluxes) by convolution with a flat-top function with a full width of 100 days and only considered the variations relative to the filtered curves (referred to as "fast" variations). The correlation results are given in the middle two rows of Table 2. Let us now suppose the typical time of change in the covering factor to be much less than the time span of 100 days then the filtering procedure will completely smooth the influence of the covering factor to its mean value. Then we must consider only the smoothed variations (referred to as "slow" variations). Their correlation coefficients are given in the last two rows of Table 2. Inspection of Table 2 shows that there is evidence for both a direct and inverse correlation. Let us consider separately each of these possibilities. If the real correlation is direct then the fast changes in EW must be attributed generally to the random changes in the covering factor to explain why they do not show the direct correlation (Table 2). If it is inverse, we must conclude that the slow changes in EW are more affected by the changes in the covering factor, and, they therefore do not show the inverse correlation (Table 2). A small coefficient value of the inverse correlation (Table 2) does not yet mean that the direct correlation is more probable. The fast variations of EW are hardly seen in the noisy measurements (Fig. 6). On the other side, the smoothed variations have much less events, since the fast changes are filtered out. Therefore, a high value of the correlation coefficient for the entire period of observations is mostly based on the fact that the strengthening of the absorption has happened at the end of our monitoring, while the continuum flux has increased systematically (Fig. 6b). However, the EW has returned almost to its initial value, while the continuum has decreased only a little.

Thus the reasons for the absorption variability are unclear. However, we definitely know that the material in the line-of-sight has undergone dramatic changes, generally during the period shown in Fig. 6c. What effects might these changes have on other absorption lines, especially on the ground-level lines with different ionization potential? We can only conclude that there is

**Table 2.** The correlation of the equivalent width of the He I $\lambda$4471 absorption line with both the optical continuum and the broad H$\beta$ emission line. The correlation coefficients are given.

| Period of observations | Comment | Correlation coefficients | | |
|---|---|---|---|---|
| | | Continuum at $\lambda$5120 | H$\beta$ line assuming no delay | H$\beta$ line assuming delay[a] |
| Entire period | | $+0.54$ | $+0.24$ | $+0.24$ |
| JD2450102–436 | | $+0.36$ | $+0.21$ | $+0.05$ |
| Entire period | Fast var. | $-0.21$ | $-0.17$ | $-0.27$ |
| JD2450102–436 | Fast var. | $-0.19$ | $-0.18$ | $-0.28$ |
| Entire period | Slow var. | $+0.73$ | $+0.37$ | $+0.38$ |
| JD2450102–436 | Slow var. | $+0.87$ | $+0.56$ | $+0.52$ |

[a] of 10 days.

no obvious evidence in favor of only-direct or only-inverse correlation of EWs with the continuum fluxes. It probably means that either the EWs are completely independent from the ionizing radiation (and then the question is Why?) or the strong changes in the covering factor (or something else) affect this link.

The blueshift of absorption lines in NGC 4151 is evidence for the predominant radial outflow of absorption gas probably located at a larger distance from the nucleus than the BLR. While the predominant motion of the absorber is a radial outflow, the BLR does not show similar kinematics (Maoz et al. 1991). So, the absorber is a distinct region rather than the outer part of BLR, or belongs to only one of the BLR components. The gaseous system responsible for the absorption contributes to the observed profiles of broad emission lines. The variations of EWs of absorption lines due to the changes in the number of clouds or in the ionizing flux can be very fast because they are formed along the line-of-sight. Although the shapes of broad-line profiles are variable even without the absorption, the absorption lines make the variations of the broad-profile shapes more complicated. In addition, the same gaseous system can produce emission lines which are slow variable because the spatial extension of this region is probably very large as compared with the "typical" BLR.

*Acknowledgements.* We are very thankful to Stanislav Kalmin for the expert and fast repairing of electronics of our CCD system which allows to carry out our observations without stopping. We are grateful to Drs. I. Savanov and V. Grinin for useful discussions.

## References

Anderson K.S., 1974, ApJ 189, 195
Anderson K.S., Kraft R.P., 1969, ApJ 158, 859
Anderson K.S., Kraft R.P., 1971, ApJ 165, L3
Bromage G.E., Boksenberg A., Clavel J., et al., 1985, MNRAS 215, 1
Cromwell R., Weymann R., 1970, ApJ 159, L147
Kaspi S., Maoz D., Netzer H., et al., 1996, ApJ 470, 336
Kriss G.A., Davidsen A.F., Blair W.P., et al., 1992, ApJ 392, 485
Kriss G.A., Davidsen A.F., Zheng W., Kruk J.W., Espey B.R., 1995, ApJ 454, L7
Leech K.J., Penston M.V., Snijders M.A.J., Gull T.R., 1987, MNRAS 225, 837
Leech K.J., Penston M.V., Snijders M.A.J., 1991, MNRAS 249, 24p
Malkov Yu.F., Pronik V.I., Sergeev S.G., 1997, A&A 324, 904 (Paper I)
Maoz D., Netzer H., Mazeh T., et al., 1991, ApJ 367, 493
Mayall N.U., 1934, PASP 46, 134
Nandra K., Pounds K.A., 1992, Nat 359, 215
Oke J.B., Sargent W.L.W., 1968, ApJ 151, 807
Peterson B.M., 1993, PASP 105, 247
Sergeev S.G., Malkov Yu.F., Chuvaev K.K., Pronik V.I., 1994, In: Gondhalekar P.M., Horne K., Peterson B.M. (eds.) Reverberation Mapping of the Broad-Line Region in Active Galactic Nuclei. ASP Conference Series 69, 199
Sergeev S.G., Pronik V.I., Malkov Yu.F., Chuvaev K.K., 1997, A&A 320, 405
Weymann R.J., Morris S.L., Gray M.E., Hutchings J.B., 1997, ApJ 483, 717